4-Junction GaAs Based Thin Film Photonic Power Converter with Back Surface Reflector for Medical Applications

Meike Schauerte[1], Oliver Höhn[1], Thorsten Wierzkowski[2], Gregor Keller[2], and Henning Helmers[1]

1) Fraunhofer Institute for Solar Energy Systems ISE, 79110 Freiburg, Germany
2) AZUR SPACE Solar Power GmbH, 74072 Heilbronn, Germany

***Abstract*—Energy supply of medical implants is a challenging task that poses requirements regarding electrical performance, safety, mechanical dimensions, biological compatibility and ideally compatibility with diagnostic methods such as magnetic resonance imaging. In this paper we report about photovoltaic cells that are optimized to power medical implants optically. We demonstrate 4-junction thin film photonic power converters (PPCs) with integrated back reflector designed to operate under monochromatic near-infrared light with a wavelength of 855 nm. The influence of the incident laser wavelength and spectral sensitivity are investigated under 809 nm and 855 nm laser light. Measurements under 855 nm light at a temperature of 25 °C suggest almost perfect current match. However, already at an operating temperature of 40 °C, as expected for operation of the implant inside the body, current mismatch becomes apparent. The impact of spectral sensitivity and current mismatch on the shape of the *I-V* curve is discussed based on measurements at a detuned wavelength of 809 nm. Furthermore, the effect of a gold back surface reflector on cell performance is examined and a lower sensitivity on current mismatch conditions due to the mirror is found. Despite the dependence of the device performance on temperature and wavelength, the maximum power point voltage remains well above 3.3 V under all relevant operating conditions, which makes these PPCs well suited to drive smart implant electronics without the need for voltage upconversion.**

Keywords—photonic power converter, thin film, III-V, multi-junction, optical power transmission, back reflector.

I. Introduction

Photonic power converters (PPCs) are photovoltaic cells that are optimized for artificial light and are used as receivers for optical power transmission systems based on a laser or a light-emitting diode. Due to the narrow light spectrum, thermalization and transmission losses in PPCs can be significantly reduced and very high light-to-electricity conversion efficiencies up to 68.9 % have been shown [1]. An optical power supply can be an elegant solution to power medical implants from outside the body. In contrast to other wireless power transmission approaches such as electromagnetic induction, optical power transmission inherently avoids electromagnetic interference. Furthermore, it is compatible with magnetic resonance imaging (MRI) tools [2] and, thus, allows to actively operate implants during MRI scans. Further advantages are that it allows to miniaturize implants [3] and increases their lifetime significantly with respect to battery powered devices [4]. A major constraint for medical implants is the compliance with biocompatibility. In this regard, release of harmful substances into the human body must be prevented. Further, heating of the tissue must be restricted to a temperature rise below 2 K, or up to 6 K under specific circumstances. For the latter reason, maximal conversion efficiency of the PPC is crucial to minimize heat dissipation from the implant.

In this work, we present 4-junction GaAs based thin film PPCs with back surface reflector (BSR), which are designed to optically power smart implants by emitting infrared light from outside of the body through the skin as depicted in Fig. 1.

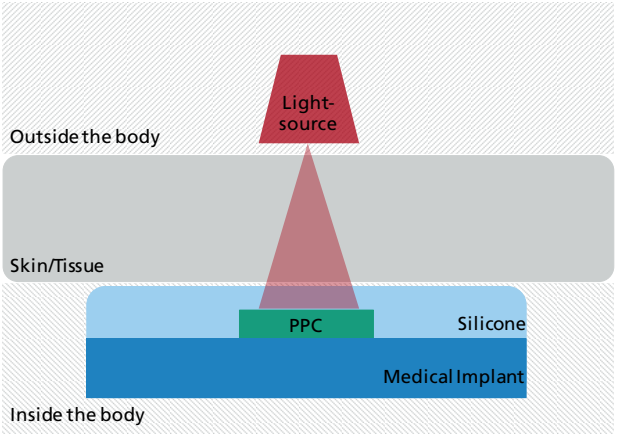

Fig. 1: A schematic view of the main components used for optical power transmission through skin/tissue to power a medical implant. The PPC can be encapsulated with e.g. silicone to assure biocompatibility.

II. Devices and Methods

A. Device Design

We fabricated vertically stacked 4-junction GaAs-based PPCs. GaAs is chosen as absorber material, as it is well suited for light absorption around 850 nm, where absorption in the tissue is low [5]. Furthermore, it can be realized with excellent material quality to enable highly efficient PPC structures.

A multi-junction device architecture [6–8] with four stacked subcells was chosen to realize an output voltage above 3.3 V as

many electrical devices and circuits are designed to operate at this voltage.

In this work, thin film cells with gold back reflector and cells on bulk substrate were fabricated and measured. The results of the following three different samples are presented here: Sample A is a reference sample processed on substrate with a wet-chemically etched mesa; the front side processing of Sample B is equal, but the substrate is removed and a gold back reflector is applied; Sample C is also processed as a thin film device with gold back reflector, but the cells were separated using a dry etching technique.

B. Epitaxial Structure

The epitaxial structure was grown by metal-organic vapor phase epitaxy (MOVPE) on 4" p-type GaAs substrates by AZUR SPACE Solar Power GmbH and is similar to the multi-junction PPC structure described in [9, 10]. A schematic of the epitaxial stack is shown in Fig. 2. The subcell thicknesses are adjusted for current matching at the target wavelength $\lambda_0 = 855$ nm at a temperature $T = 25$ °C. The four stacked subcells are electrically interconnected in series by tunneling diodes (TD). A 1 µm thick transparent lateral conduction layer on the front side facilitates carrier transport to the metal front grid [11]. Between the stacked subcells and the substrate, an etch stop layer is introduced to enable selective removal of the substrate by wet chemical etching during the thin film processing scheme.

C. Semiconductor Processing

After epitaxy of the semiconductor structure, the device processing was performed in the Fraunhofer ISE cleanroom laboratory, following a processing scheme similar to the one described in [12]. First, a full area rear side contact metallization based on Pd/Zn/Pd/Au was applied to the reference sample on substrate. The Pd/Au/Ge/Ti/Pd-based front side contacts were realized by metal evaporation and liftoff processes. The front contact layer between the metal fingers was removed by a selective etching step using a citric acid:H_2O_2 solution. Mesa etching was performed using a non-selective HBr:H_2O_2:H_2O solution for a defined time, followed by selective etching of the last layers with a citric acid:H_2O_2 solution. Alternatively, a dry etch step based on reactive ion etching was applied. Finally, an anti-reflection coating (ARC) was deposited by physical vapor deposition. For laboratory testing in air atmosphere a two-layer ARC made of Ta_2O_5 and MgF_2 optimized for the wavelength range from 800 nm to 870 nm was evaporated. PPCs of two different sizes were fabricated with nominal designated areas of 0.054 cm² and 0.61 cm².

For thin-film processing, the wafers with finished front-side but without rear side contact, were temporarily bonded to a sapphire wafer, similar to the process described in [12]. Then, the GaAs substrate was selectively removed using a NH_4:H_2O_2:H_2O solution. The wet chemical etching stops at the etch stop layer which is consecutively removed with HCl. After substrate etching, the rear side contact layer of the PPC was covered with thermally evaporated gold which serves as a BSR and electric contact at the same time. Subsequently, the rear side is reinforced by 15 to 30 µm of electroplated copper. Finally, the temporary bond is released, and flexible thin film wafers are obtained (see Fig. 3).

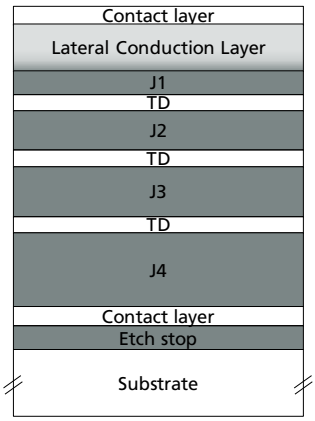

Fig. 2: Schematic cross section of the epitaxial structure of the 4-junction PPCs. Subcells 1 to 4 (J1-J4) are decreasing in thickness from top to bottom and are interconnected by tunneling diodes (TD).

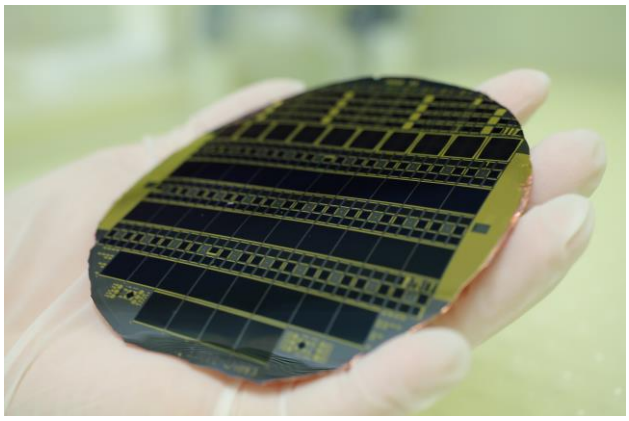

Fig. 3: The picture shows a fully processed flexible thin film wafer with gold back reflector.

D. Characterization

Current-voltage (*I-V*) measurements were performed on 0.61 cm² cells on a temperature-controlled chuck at $T = 25$ °C under 809 nm laser light and at $T = 25$ °C and $T = 40$ °C under a 855 nm light source. For both measurements the best cell on each wafer was chosen based on flash measurements with broadband light. In both cases the voltage sweep to obtain the *I-V* characteristic was performed within 1 ms. *I-V* characteristics were measured in forward and backward direction, i.e. the voltage was swept from negative bias to beyond open-circuit and the other way around. The data was logged using a transient recorder. The optical input power was determined by using a single-junction GaAs reference cell with the same cell area and the same metal grid shading as the device under test (DUT). The short circuit current I_{SC} of the reference cell was measured separately under the same irradiance conditions as the DUT before the series of measurements. The input power P_{in} was calculated using the calibrated spectral response of the reference cell.

In case of measurements with the 809 nm laser, the light emitted from a DILAS MINI Diode Laser System was guided through an optical fiber and directed onto the DUT. An aperture mask was used to assure that the cells are slightly under-illuminated. The cells were aligned with the help of a visible 650 nm pilot laser coupled into the same fiber. The optical input power was varied over three orders of magnitude from 0.18 W to 13.8 W. To obtain the *I-V* characteristics, a 4 ms-laser pulse is triggered manually, and the voltage sweep starts after a delay time of 1.9 ms.

Electrical characterization at 855 nm, which is the wavelength of intended current matching, was performed using a vertical-cavity surface-emitting laser (VCSEL). Its peak wavelength is 855 nm and it has a full width at half maximum of 2 nm. To align the DUT with respect to the VCSEL light spot the following procedure was executed: The photo current of the DUT was estimated by measuring the voltage drop over a 1 kΩ resistor. By moving the cell in the x- and the y-direction in 0.5 mm steps, the point of maximum photo current was determined. The *I-V* measurement was then executed at this position for different input powers ranging from 83 mW to 511 mW. For these measurements the delay time between starting the laser and the start of the measurement was increased to 2 s.

Note, that for both laser light sources the intensity is not distributed homogeneously across the active cell area, but rather features radial symmetry with peak intensity at the center of the cell. For that reason, the total optical input power [W] is reported for the measurements, instead of the irradiance [W/cm²].

III. Results and Discussion

For both measurement setups a hysteresis between forward and backward voltage sweep especially strong at low irradiances was observed. The effect was found to be less pronounced for slower voltage sweeps and is hence attributed to capacitive effects in the 4-junction device. However, the *I-V* curves shown in the following show the average current of the forward and backward measurement for each voltage sampling point. An analysis of different methods to average the forward and the backward *I-V* is currently under investigation. Comparison of data acquired with different sweep times and, thus, different severeness of the hysteresis effect showed that this averaging yields reliable values for open circuit voltage V_{OC} and the short circuit current I_{SC}, but usually underestimates the fill factor *FF* due to a rounding artifact in the averaged *I-V* curve around the maximum power point.

A. Measurements under 809 nm light

Fig. 4 shows *I-V* curves of 0.61 cm²-sized PPCs measured at different input powers ranging from 0.18 W to 13.8 W for all three samples (Sample A on substrate with wet-chemical mesa etching, Sample B with gold back reflector, and Sample C with gold Back reflector and dry mesa etching). At voltages around 0 V for all *I-V* curves a bending is observed, so that the short-circuit current is significantly larger than the "saturated" current between about 1 V and 4 V. This behavior can be understood as follows: As the subcells' thicknesses are optimized for

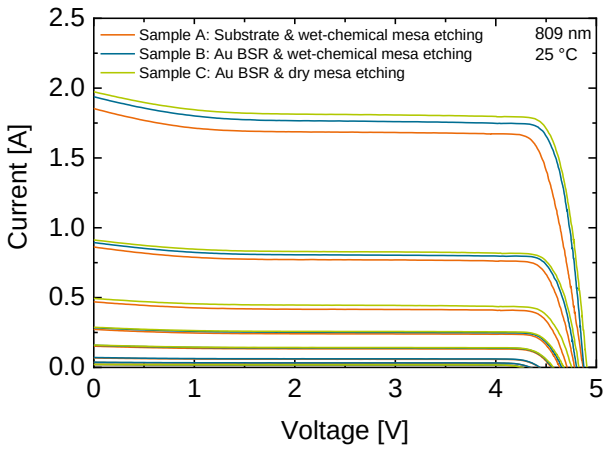

Fig. 4: Measured current-voltage characteristics of PPCs on substrate and with gold back reflector measured under 809 nm laser light with different intensities. The current and the open circuit voltage are higher for the cells with back surface reflector. Sample B was not measured at the 3rd highest irradiance.

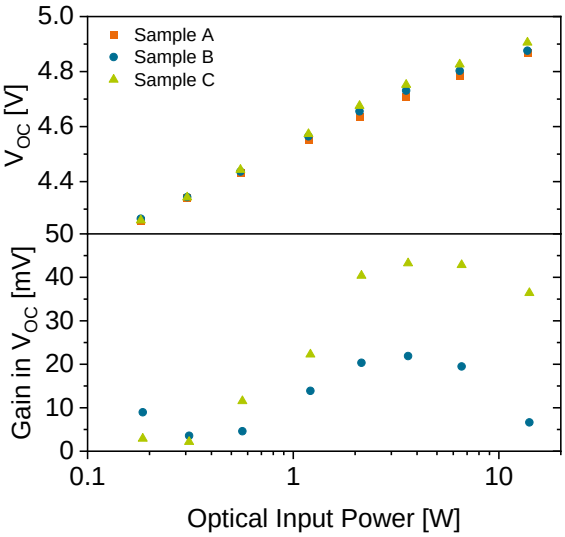

Fig. 5: Top: Open circuit voltage V_{OC} as a function of input power extracted from the *I-V* measurements. Bottom: Gain in V_{OC} attributed to the back surface reflector (Gain = V_{OC}(Sample B/C) – V_{OC}(Sample A)). At low irradiances the V_{OC} is similar for all samples. With increasing irradiance, a gain in V_{OC} for the samples with mirror is observed. Sample C with a dry etched mesa shows a higher V_{OC} gain than the wet etched sample. When the irradiance is increased further, the gain starts decreasing due to the heating of the thin film cells.

current matching at $\lambda_0 = 855$ nm, the multi-junction structure is current mismatched when measured under 809 nm light. More precisely, the subcells' generated photocurrent densities decrease from top to bottom due to the increased absorptance at lower wavelengths [13, 14]. As the junctions are connected in series, the bottom (J4) subcell's photo current is limiting the overall current of the device. At voltages above ~1 V J1-J3 are operating close to their respective single subcell open circuit voltages, which are in first order approximation equal to one quarter of the device's V_{OC}. Hence, the limiting junction is at zero voltage bias when the externally applied voltage is approximately $V = 3/4\ V_{OC}$. More generally speaking, the

limiting junction in a mismatched multi-junction device is estimated to operate at zero voltage bias when $V = (N\text{-}1)V_{OC}/N$, with V_{OC} being the multi-junction open circuit voltage and N the number of subcells. Consequently, when the external bias voltage approaches $V = 0$ V, the limiting bottom junction J4 operates already in significant negative bias. The bending at an external voltage of about 1 V, thus, is interpreted as a reverse breakdown of the limiting junction, so that the *I-V* curve bends up to the photocurrent of the next limiting junction.

At all irradiances, the current is higher for the cells with back surface reflector which is attributed to improved luminescent coupling due to the mirror.

Fig. 5 shows the measured open circuit voltages as a function of optical input power and the gain in V_{OC} attributed to the back surface reflector. The V_{OC} increases logarithmically with optical input power. A gain in V_{OC} due to the Au reflector of up to 22 mV for the wet chemically separated cell and of up to 43 mV for the cell with dry etched mesa is observed. In both cases, the gain is attributed to more effective photon recycling in the bottom subcell as well as improved luminescence coupling and a thereby increased current. The higher open circuit voltages and the higher currents for sample C indicate that the dry mesa etching process is advantageous for these multi-junction PPCs. For the highest measured input powers the gain in V_{OC} drops which is attributed to worse thermal coupling of the flexible wafers to the measurement chuck and, thus, more pronounced heating of the DUT during measurement at such high irradiance; similar as observed in other measurements [1].

B. Measurements under 855 nm light

Fig. 6 shows a comparison of *I-V* curves of cells with and without back reflector (samples A and B, same cells as shown in Fig. 4) measured under 855 nm light. The measurements were performed under different optical input powers between 83 mW to 511 mW. At low powers nearly identical characteristics are found for the cells with and without mirror. At higher powers a small deviation can be observed between the two samples. The bending in the *I-V* curve of the thin film cell indicates a slight current mismatch. We attribute this, as for the 809 nm measurements, to a worse thermal coupling of the thin-film wafer to the measurement chuck. Namely, the cells heat up during the 2 s of laser illumination before the measurement starts.

Fig. 7 illustrates the effect of increasing temperature on the I-V curve. It shows measurements of sample A (on substrate) at $T = 25$ °C (black lines) and $T = 40$ °C (red lines). The increase in temperature leads to a drop in V_{OC} of 116 to 131 mV (-1.93 to -2.18 mV/K per junction). The bending of the current around $V = 0$ V for the 40 °C measurement indicates a temperature induced current mismatch due to the enhanced absorptance in the top subcells.

A direct comparison of *I-V* curves of the same cell measured under 809 nm and 855 nm is shown in Fig. 8. Both *I-V* curves were measured the same optical input power, namely 181 mW. Note that the measured voltage range covers negative bias voltages reaching as low as -13 V. The *I-V* curve measured at 855 nm (black line) is rather flat throughout the whole voltage range, apart from a small bending around $V = -7.5$ V and

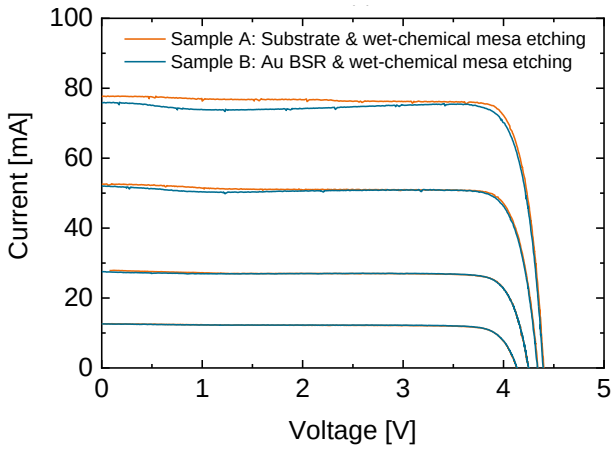

Fig. 6: I-V characteristics of a cell on substrate (sample A, orange curves) and a cell with gold back reflector (sample B, blue curves) for different optical input powers (83, 181, 344 and 511 mW from bottom to top) at 855 nm. For the lower intensities the cells with and without mirror show similar behavior. The difference at higher intensities is caused by the more pronounced heating of the thin-film cell due to worse thermal coupling to the measurement chuck.

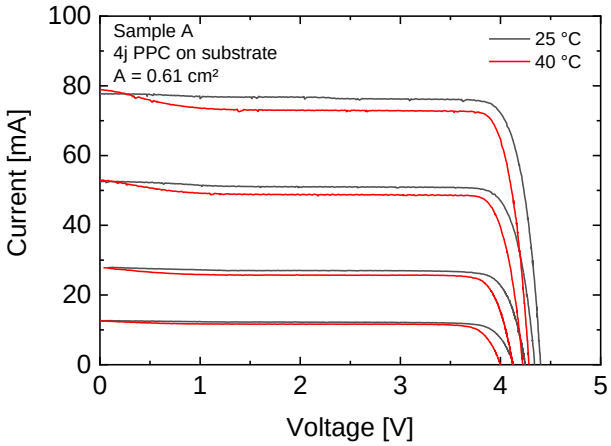

Fig. 7: *I-V* characteristics of a cell on substrate for different chuck temperatures (25 °C, black lines and 40 °C, red lines) and different optical input powers measured under the VCSEL emitting at 855 nm. For higher temperatures, a reduction in V_{OC} is observed and the current shows a bending at $V = 0$ V, indicating a small current mismatch.

another around $V = -13$ V. For the measurement under 809 nm (red line), however, the I-V curve exhibits distinct steps of stable current with transition ranges in between. The bending is observed at around $V = +1$ V, -4.5 V, -9 V and -15 V (outside of the measurement range in Fig. 8). These distinct steps in the *I-V* curve can be understood by the series connection of the subcells which each generate a different photo current: The combined *I-V* curve of a string of series connected cells is determined by the sum of the voltages for each current value. Due to the strong current mismatch, the liming junction (here: J4) is already in reverse bias at zero external bias voltage. Further decrease of the external bias, thus, drives the limiting junction further in reverse, and the *I-V* characteristic is determined by its breakdown behavior. At around -2.5 V the photocurrent of the second limiting junction is reached, which then determines the current as long it does not break down while voltage is further decreased. As a consequence, four

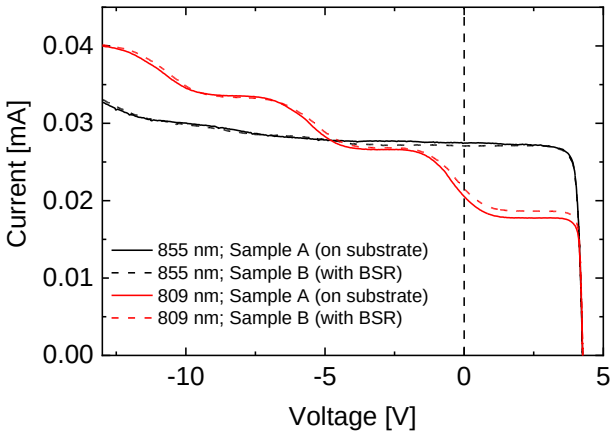

Fig. 8: *I-V* characteristics of sample A (straight lines) and sample B (dashed lines) measured at 809 and 855 nm at the same optical input power (P_{in} = 181 mW) are shown. In case of the measurement at 809 nm (red lines), four different plateaus corresponding to the subcells' short-circuit currents can be observed. For the cell with back surface reflector (sample B) a higher current is observed in the current plateau corresponding to the short circuit current of the bottom junction ($I_{sc,4}$) due to improved luminescent coupling from the current over-producing top subcells to the bottom subcell. Measured under 855 nm (black lines), the cells show close to current-matched behavior with only one small current plateau corresponding to one slightly more absorbing subcell.

distinct plateaus emerge which each represent the photo current of one of the subcells. Finally, at even further decreased bias voltage also the last junction and, thus, the entire device is expected to break down, which happens in this case at a voltage below the measurement range.

The comparison of these two measurements clearly reveals how current mismatch (or alternatively spectral mismatch by using a detuned wavelength) affects vertically stacked multi-junction PPCs. Especially the photo current of the limiting bottom cell and consequently the current at maximum power point is severely affected by spectral mismatch. As can be seen in Fig. 8, the back surface reflector increases the photo current in the limiting bottom subcell, whereas the upper subcells show similar photo currents in both cases. This can be understood, as the back reflector enhances the effect of luminescence coupling from the top subcells towards the bottom subcell, because it effectively increases its optical thickness and thus increases the absorptance of the otherwise only weakly absorbed near-bandgap photons emitted from the upper subcells. In this measurements, the detuning of the laser wavelength by 46 nm leads to a drop in current at maximum power point I_{mp} from 25.1 mA to 16.3 mA (-35 $\%_{rel}$), i.e. 0.76 $\%_{rel}$ per 1 nm spectral mismatch, that translates into a similar drop in efficiency. The introduction of a back surface reflector mitigates the loss in current to -32 $\%_{rel}$ (or 0.7 $\%_{rel}$ per 1 nm spectral mismatch) due to improved luminescence coupling even at the low input power of 181 mW (0.3 W/cm²). At higher optical input powers, a more pronounced effect is expected. Still, it should be noted that these average numbers were derived from measurements at two wavelengths only while the actual behavior with spectral detuning generally would be expected to be non-linear. Last, it is emphasized that these observations and given explanations are in line with previous studies and conclusions regarding the operation of multi-junction PPCs [7, 15].

IV. Conclusion

We fabricated and characterized 4-junction GaAs-based PPCs with and without back reflector. The devices were developed to power smart implant applications by infrared light beaming through tissue. With these devices the voltage at the maximum power point exceeds 3.3 V even at low intensities so that implants can be powered without the need of voltage upconversion.

It was shown that changes in the operating temperature induce significant current mismatch among the subcells causing a loss in current by -0.76 $\%_{rel}$/nm. By implementing a gold back reflector this current drop reduces to -0.7 $\%_{rel}$/nm. This finding underlines the importance of careful design and epitaxial growth with respect to the light source and operating temperature. In addition to performance benefits from the thin film approach with back mirror, the resulting flexibility of the devices is advantageous for the integration into curved surfaces or foil substrates. Due to these advantages, such thin-film devices can unlock the ability to power medical applications by infrared light.

Acknowledgment

The authors thank R. Freitas, R. Koch, C. Kopiniok, G. Mikolasch, for processing support; and F. Dimroth, E. Oliva, F. Predan, M. Schachtner, G. Siefer, J. Wulf for valuable discussions. Also, we thank W. Luppold at Fraunhofer IAF for dry etchingsupport. This work was funded by the German Federal Ministry of Education and Research (BMBF) through the project "Lightbridge" (16ES0788).

References

[1] H. Helmers, E. Lopez, O. Höhn, D. Lackner, J. Schön, M. Schauerte, M. Schachtner, F. Dimroth, and A. W. Bett, "68.9% Efficient GaAs Based Photonic Power Conversion Enabled by Photon Recycling and Optical Resonance," *physica status solidi – Rapid Research Letters*, vol. in press, 2021.

[2] S. Ayazian and A. Hassibi, "Delivering optical power to subcutaneous implanted devices," (eng), *Conference proceedings : Annual International Conference of the IEEE Engineering in Medicine and Biology Society.*, vol. 2011, pp. 2874–2877, 2011.

[3] A. Ahnood, R. Cheriton, A. Bruneau, J. A. Belcourt, J. P. Ndabakuranye, W. Lemaire, R. Hilkes, R. Fontaine, J. P. D. Cook, K. Hinzer, and S. Prawer, "Laser Driven Miniature Diamond Implant for Wireless Retinal Prostheses," (eng), *Adv. Biosyst.*, e2000055, 2020.

[4] C. Algora and R. Peña, "Recharging the battery of implantable biomedical devices by light," *Artif. Organs*, vol. 33, no. 10, pp. 855–860, 2009.

[5] T. Lister, P. A. Wright, and P. H. Chappell, "Optical properties of human skin," (eng), *J. Biomed. Opt.*, vol. 17, no. 9, 90901-1, 2012.

[6] J. Schubert, E. Oliva, F. Dimroth, W. Guter, R. Löckenhoff, and A. W. Bett, "High-Voltage GaAs Photovoltaic Laser Power Converters," *IEEE Trans. Electron Devices*, vol. 56, no. 2, pp. 170–175, 2009.

[7] E. Lopez, O. Höhn, M. Schauerte, D. Lackner, M. Schachtner, S. K. Reichmuth, and H. Helmers, "Experimental coupling process efficiency and benefits of back surface reflectors in photovoltaic multi‐junction photonic power converters," *Prog. Photovolt: Res. Appl.*, vol. 29, no. 4, pp. 461–470, 2021.

[8] S. Fafard, F. Proulx, M. C. A. York, L. S. Richard, P. O. Provost, R. Arès, V. Aimez, and D. P. Masson, "High-photovoltage GaAs vertical

epitaxial monolithic heterostructures with 20 thin p/n junctions and a conversion efficiency of 60%," *Appl. Phys. Lett.*, vol. 109, no. 13, p. 131107, 2016.

[9] AZUR SPACE Solar Power GmbH, *Laser Power Converter Diode Type LPC-810-x-00:* Datasheet available at http://azurspace.com/images/DB_0005417-02-00_LPC-810-x_LaserPowerConverter.pdf

[10] G. Keller, D. Fuhrmann, T. Wierzkowski, A.-K. Volk, B. Fuhrmann, L. Horst, C. Wächter, M. Schauerte, H. Helmers, and V. Khorenko, "GaAs Multi-Junction Laser Power Converters at AZUR SPACE: Current Status and Development Activities," in *Technical Digest of the 1st Optical Wireless and Fiber Power Transmission Conference (OWPT2019)*, Yokohama, Japan, 2019, pp. 11–12.

[11] E. Oliva, F. Dimroth, and A. W. Bett, "GaAs Converters for High Power Densities of Laser Illumination," *Prog. Photovolt: Res. Appl.*, vol. 4, no. 16, pp. 289–295, 2008.

[12] C. L. Schilling, O. Höhn, D. N. Micha, S. Heckelmann, V. Klinger, E. Oliva, S. W. Glunz, and F. Dimroth, "Combining Photon Recycling and Concentrated Illumination in a GaAs Heterojunction Solar Cell," *IEEE J. Photovolt.*, vol. 8, no. 1, pp. 348–354, 2018.

[13] H. Helmers, L. Wagner, C. Garza, S. Reichmuth, E. Oliva, S. P. Philipps, D. Lackner, and A. W. Bett, "Photovoltaic Cells with Increased Voltage Output for Optical Power Supply of Sensor Electronics," in *Proceedings SENSOR 2015*, Nürnberg, Germany, 2015, pp. 519–524.

[14] S. P. Philipps, D. Stetter, R. Hoheisel, M. Hermle, F. Dimroth, and A. W. Bett, "Characterization and numerical modeling of the temperature-dependent behaviour of GaAs solar cells," in *Proceedings of the 23rd European Photovoltaic Solar Energy Conference*, Valencia, Spain, 2008, pp. 114–117.

[15] S. K. Reichmuth, H. Helmers, S. P. Philipps, M. Schachtner, G. Siefer, and A. W. Bett, "On the temperature dependence of dual-junction laser power converters," *Prog. Photovolt: Res. Appl.*, vol. 25, no. 1, pp. 67–75, 2017.